Impact of 3D Fields on Divertor Detachment in NSTX and DIII-D

J-W. Ahn[1], R.E. Bell[2], A.R. Briesemeister[1], J.M. Canik[1], A. Diallo[2], T.E. Evans[3], N.M. Ferraro[3], S.P. Gerhardt[2], B.A. Grierson[2], T.K. Gray[1], S.M. Kaye[2], M.J. Lanctot[3], B.P. LeBlanc[2], J.D. Lore[1], R. Maingi[2], A.G. McLean[4], D.M. Orlov[5], T.H. Osborne[3], T.W. Petrie[3], A.L. Roquemore[2], F. Scotti[4], O. Schmitz[6], M.W. Shafer[1], V.A. Soukhanovskii[4], E.A. Unterberg[1], and A. Wingen[1]

[1]*Oak Ridge National Laboratory, Oak Ridge, TN 37831, USA*

[2]*Princeton Plasma Physics Laboratory, Princeton, NJ 08543, USA*

[3]*General Atomics, P.O. Box 85608, San Diego, CA 92186, USA*

[4]*Lawrence Livermore National Laboratory, Livermore, CA 94551, USA*

[5]*University of California – San Diego, La Jolla, CA 92093, USA*

[6]*University of Wisconsin – Madison, Madison, WI 53706, USA*

Email: jahn@pppl.gov

Abstract. Divertor gas puff was used to create detached divertor condition and the effect of 3D fields on the detachment was investigated for H-mode plasmas in NSTX. The divertor remains partially detached with the 3D field application when sufficient amount of gas is injected into the divertor region, which is accompanied by a noticeable drop of pedestal electron temperature (T_e). However, with a lower gas puff, the divertor plasma re-attaches, when 3D fields were applied to the detached plasma, and the pedestal T_e rises back up. There observed no other change in the pedestal profile associated with the re-attachment, indicating that this is likely to be dominated by a change in the electron thermal transport processes. A TRANSP analysis shows that the drop of pedestal electron heat diffusivity (χ_e) is responsible for this change but the cause of this reduction is yet unclear. A similar experiment was conducted at DIII-D but the plasma response induced strong screening to mask separatrix splitting that led to almost no impact on detachment. It is shown that plasma triangularity (δ) plays an important role in the formation of separatrix splitting via kink response in connection with the parallel edge current.

1. Introduction

Understanding and modeling divertor plasmas is pivotal for optimizing the design of future fusion reactors where large heat loads will need to be reliably distributed. 3D fields may be used to suppress or mitigate ELMs in ITER where it will be also necessary to achieve detachment to control steady state heat loads on the divertor plates. It is therefore important to understand what effects 3D fields have on detachment. It has been shown in NSTX [1] that 3D fields increase the amount of gas needed to achieve divertor detachment. Similar results were seen in DIII-D, where despite causing a reduction in the pedestal density, applying 3D fields promoted attachment of the inner divertor leg [2]. The mechanisms causing these changes are not well understood. However, a well-known result of applying 3D magnetic perturbation to diverted tokamak plasmas is the formation of striations in the particle and heat fluxes to the divertor, giving spiraling flux patterns on the plasma facing component (PFC) surface. This is attributed to the splitting of the separatrix into stable and unstable manifolds [3], which have a helical lobe structure that is pronounced near the X-point and can intersect the PFCs resulting in the observed striations. Understanding and predicting plasma transport

along these magnetic structures is necessary for future devices such as ITER to avoid significant fluxes in unexpected locations.

Modifications to the ion flow structure are among the changes that are predicted to occur in response to applied 3D fields. On the open field lines within the divertor large flow velocities can develop as a result of the Bohm sheath criterion at the plasma/wall interface [4]. 3D fields may lead to the formation of magnetic lobe structures which alter the connection length to the divertor targets [5]. In response to these magnetic perturbations closely spaced regions of counter streaming flows are predicted to form [6] and change the ion transport within the divertor that could potentially impact detachment onset. A similar phenomenon occurs in stellerators due to the geometric effect of the magnetic island divertor which causes enhanced downstream momentum loss [7].

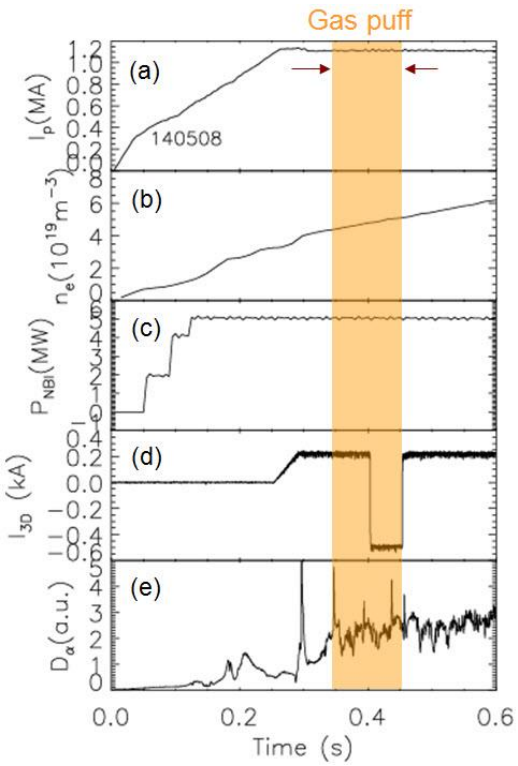

Figure 1 Time trace of (a) plasma current, (b) line average density, (c) NBI power, (d) 3D field coil current, and (e) divertor D_α signal, taken during a divertor detachment and 3D field application experiment in NSTX. The n=3 perturbation fields are superimposed onto the n=3 error correction fields for the 2nd half (t=0.4 – 0.45 sec) of the detachment period (t=0.35 – 0.45 sec, orange shadow).

The compact size of the spherical tokamak (ST) geometry naturally leads to more serious heat flux problem for a given heating power and plasma current. This is true for both the steady state and the transient ELM heat deposition. Therefore, the ELM control using the 3D fields and the peak heat flux reduction technique with the divertor detachment must be compatible. Partial divertor detachment both on the inboard and outboard sides has been demonstrated in the high performance H-mode plasmas in NSTX [8]. Results from NSTX have shown that partially detached divertor plasma can be re-attached by applying 3D fields (n=3) [1]. However, this can be avoided when the detachment is enhanced by puffing sufficient gas into the divertor region. A similar experiment performed at DIII-D demonstrated the importance of plasma response to the applied 3D fields in inducing separatrix splitting and therefore its impact on divertor detachment. Data from NSTX will be presented in sections 2 and 3, while results obtained at DIII-D will be described in section 4.

2. Experimental approach and effect of 3D fields on divertor plasma in NSTX

Figure 1 shows the time trace of several plasma parameters. A large amount of deuterium (D_2) gas is puffed into the lower divertor area through the 'CHI gap' between the inner and outer divertor plates, for naturally ELMy H-mode plasmas to produce partially detached divertor condition, *i.e.* detachment only occurs near the strike point. A small amount of lithium (50 mg for the inter-shot evaporation, compared to ~300 mg necessary for the full ELM suppression) was used to condition the PFC surface. The orange shaded period in figure 1 represents the time of D_2 injection. Panel 1(d) is the time trace of a 3D coil current. 0.2kA of n=3 error field correction field is applied first and then the n=3 perturbation field is superimposed for the 2nd half of the gas puff period. The amplitude of 3D coil current (I_{3D} = −

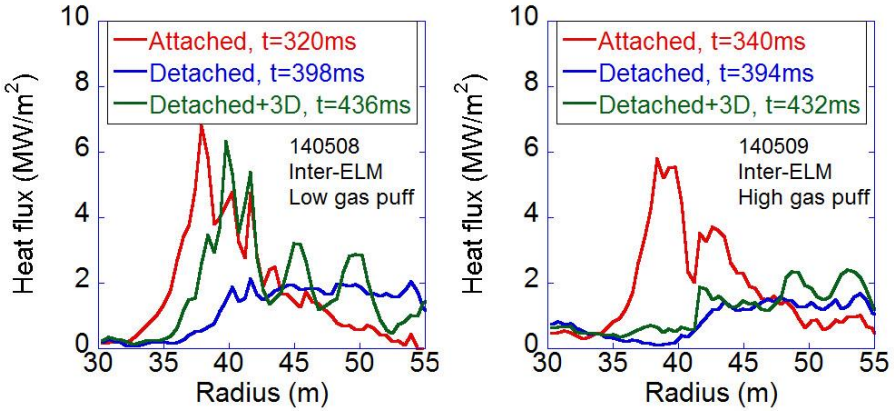

Figure 2 Measured heat flux profiles in NSTX for discharges with divertor detachment by (a) low and (b) high divertor gas puff (D_2). Each profile is color coded; red is before gas puff, blue is after gas puff, green is after gas puff plus 3D field application.

0.5 kA) is below the ELM triggering threshold that was confirmed from the ELM triggering experiment in the lithium enhanced ELM-free plasma. Plots in figure 2 are the calculated heat flux profile onto the divertor surface during the inter-ELM period, based on the dual band IR camera data. Two levels of gas amount for the divertor puff were tested. Plot 2(a) is for the low gas puff (2000 Torr of pressure, estimated to be ~$7x10^{21}$ D/sec of particle flow rate) and 2(b) is for the high gas puff (3000 Torr of pressure, estimated to be ~$11x10^{21}$ D/sec of flow rate) case. Heat flux profiles in red are before the gas puff and are peaked near the strike point at r~38 cm in both cases, which indicates that the divertor plasma is attached. The blue profiles are obtained after the detachment onset (by gas puff) but before the 3D field application. The peak heat flux is reduced by ~70 % compared to those in the attached regime before the gas puff. It is also seen that the heat flux profile after the detachment onset is slightly higher for the low gas puff case. This is interpreted as a "weaker" detachment compared to the high gas puff case. The green profiles are after the 3D field was applied to the detachment. It is clearly seen that the heat flux profile becomes peaked again in the low gas puff case; the divertor plasma re-attaches. However, it stays flat in the high gas puff case, which indicates that the plasma remains detached. Therefore, the 3D fields can re-attach weakly detached plasma but this can be avoided by enhancing detachment with higher gas puff.

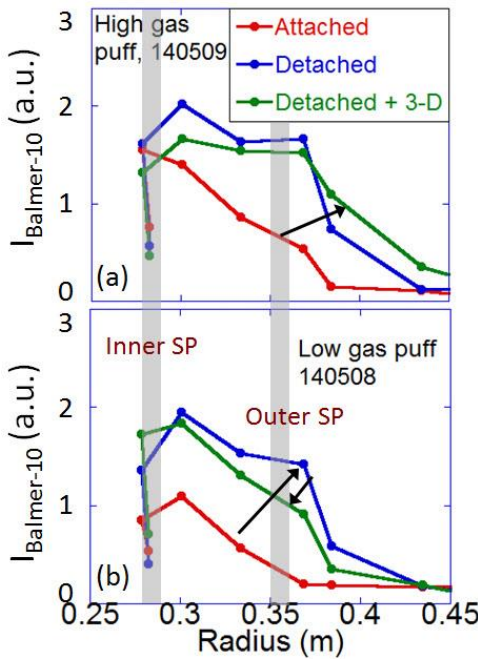

Figure 3 Radial profile of Balmer-10 emission intensity in NSTX for (a) high gas puff and (b) low gas puff case. Each plot shows data for three time slices; before gas puff (red, attached), during gas puff (blue, detached), and 3D field applied during gas puff (green, re-attached). The location of inner and outer strike points (SPs), from EFIT, is shown by the grey vertical bars. The arrows indicate that the profile continues to grow in the (a) high gas puff case and the width reverts with the onset of re-attachment in the (b) low gas puff case.

The evidence of detachment by divertor gas puff and re-attachment induced by the applied 3D fields is also provided by spectroscopic data. High-n Balmer line emission, for example Balmer-10, provided by DIMS diagnostic [9] is a good indicative of volume recombination and is only present in the condition of low T_e (< 5 eV) and high density. We thus use this signal as an indicator of divertor plasma condition. Figure 3 shows the radial distribution of line integrated Balmer-10 line emission intensity for the high and low gas puff

cases. The radius values here represent radii of the intersection of poloidal chords of DIMS diagnostic with the divertor surface. The location of inner and outer strike points is also overlaid in figure 3. Note that the poloidal chords are line integrated so that data are not only for the strike points but also contain contributions from regions above the divertor surface including the X-point region. The inner strike point almost always detaches in NSTX [8], and this is demonstrated in both figures 3(a) and 3(b) that the Balmer-10 intensity near the inner strike point is peaked even before the gas puff stage (the red profiles), while the intensity near the outer strike point remains low. With the gas puff, intensities near the outer strike point rapidly increases, leading to the broadening of the emission profile (blue profiles). This continues to grow after the application of 3D fields in the high gas puff case, figure 3(a), but with the onset of re-attachment by 3D fields in the low gas puff case, figure 3(b), the process begins to reverse (green profiles). This observation is consistent with the temporal evolution of surface heat flux profiles shown in figure 2.

3. Effect on the pedestal plasma in NSTX

3.1 Background study for the attached divertor plasma

This sub-section is intended to review previous NSTX results in the attached condition in comparison with the data in the detached condition to be presented in section 3.2. As described in the introduction section, 3D fields not only modify divertor footprints but also change the pedestal profiles in NSTX [10,11,12]. However, the effect is less consistent compared to the robust strike point splitting observed in the divertor plasma, as explained below. Comparison of pedestal profiles before and after the 3D fields (n=3) without the use of lithium PFC coating show the increase of T_e gradient by 3D fields while n_e remains almost unchanged. A modified tanh fitting gives ~30 % increase in the peak edge pressure gradient (∇p_e) caused by this increase [10,11]. The increase of ∇p_e was calculated to be sufficient to destabilize peeling-ballooning modes, which is consistent with the triggering of large ELMs observed in NSTX [10]. Note that T_i profile decreases only modestly but the drop of overall V_t profile after n=3 is quite significant.

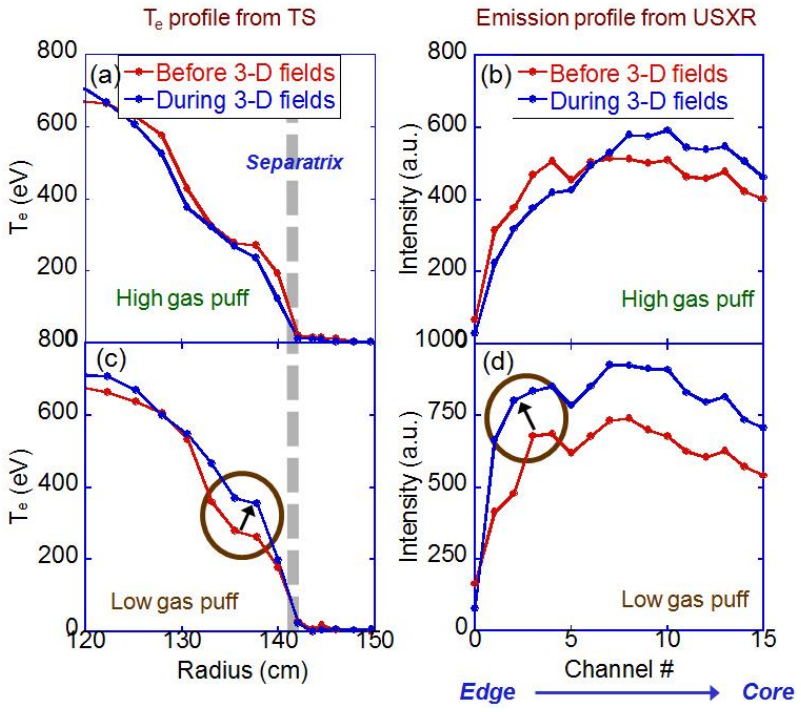

Figure 4 Pedestal T_e profile (left column) and poloidal USXR channel signals (right column) in NSTX. The upper row (figures (a) and (b)) is for high gas puff and the lower row (figures (c) and (d)) is for the low gas puff, with 3D fields applied later during the detached phase in both cases.

When lithium coating was used to produce ELM-free H-mode plasmas, however, the effect of the applied 3D fields on the pedestal plasma is not the same as the case without lithium described above. A flattening in both the T_e and n_e profiles in the region of Ψ_N ~ 0.8–0.9 is observed [12], where Ψ_N is

the normalized poloidal flux. In other words, the rise of pressure gradient reported in [10,11] does not occur in this case. However, ELMs are still triggered as a result of edge destabilization after the application of n=3 fields. This suggests that the mechanism of ELM triggering may not be limited to the increase of edge pressure gradient but can be attributed to another cause. The change in the T_i and V_t profiles is similar to that observed in the case of no lithium coating. A field line tracing from the SIESTA magnetic field modeling [12] was carried out to compare to the experimental observation. The SIESTA code [13] can generate a quasi-resistive equilibrium allowing for the possibility of magnetic island formation. It revealed the magnetic island overlap in the radial region similar to where the flattening of T_e and n_e is observed, *i.e.* Ψ_N ~ 0.8–0.9. However, the electron thermal and particle diffusivity due to stochastic transport using the SIESTA magnetic field are much lower than the values inferred from the SOLPS 2-D edge modeling using the observed profile data [12].

3.2 Effect on the pedestal plasma with divertor detachment

As the detachment of divertor plasma is established, the pedestal T_e progressively drops with increasing gas puff, while the pedestal n_e changes only little. The T_i and V_t profiles also decrease only modestly in the overall pedestal region with the onset of detachment. Therefore, the pedestal T_e drop is most prominently observed in NSTX when the divertor plasma detaches, which also leads to the reduction of pedestal electron pressure, $p_{e,ped}$. Figure 4 illustrates the effect of 3D fields on the pedestal plasma with detachment. Panels 4(a) and 4(c) are the mid-plane T_e profiles and 4(b) and 4(d) are the emission profiles from the USXR array. The upper row, panels 4(a) and 4(b), is for the high gas puff and the lower row, 4(c) and 4(d), is for the low gas case. In the continued detachment with high gas puff, the pedestal T_e profile remains decreased before and after turning on the 3D field, so the applied 3D field has no effect on the T_e profile, figure 4(a). It is also seen in figure 4(b) that the USXR data for the edge channels continuously decrease. On the other hand, in the case of re-attachment, the pedestal T_e rises back up after the application of 3D fields, see figure 4(c). The increase is usually by ~100 eV and the edge soft X-ray data also shows increase, figure 4(d). As the pedestal n_e does not change significantly as explained above, this increase of edge USXR is attributed to the increase of pedestal T_e. It is noted that the T_i and V_t data in the pedestal region are not affected by the applied 3D fields even for the re-attachment case (see figure 5). This implies that the physical mechanism responsible for the divertor detachment and re-attachment is likely to be carried out by the change in electron thermal transport process. The observation of $T_{e,ped}$ increase and the unchanged $n_{e,ped}$ with the application of n=3 fields is consistent with the previous result in NSTX without the use of lithium PFC coating referenced in section

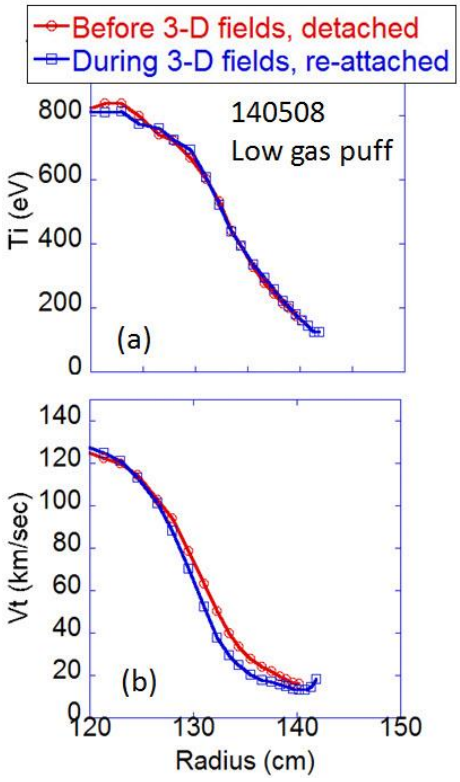

Figure 5 Pedestal T_i (a) and V_t (b) profiles before (red) and after (blue) the n=3 fields application in NSTX in the low gas puff case, during which divertor re-attachment was induced.

3.1, reported in [10,11,12]. Note that we only used a minimal amount of lithium for the detachment experiment presented in this paper in order to keep ELMs, therefore these data should be compared to the case with no lithium in [12]. The observed $T_{e,ped}$ increase in case of re-attachment is found to be associated with the change in global parameters too. For example, the total radiation power (P_{rad}) usually decreases during the detached phase but it rose back up when the plasma re-attached by 3D fields.

In an effort to explain how the observed $T_{e,ped}$ change was induced, a TRANSP [15] modeling was carried out for these discharges using the measured T_e and n_e profiles as input, and figure 6 shows the pedestal electron heat diffusivity (χ_e) profiles. The derivation of χ_e is based on the electron energy conservation equation as follows,

$$\frac{d}{dt}\left(n_e T_e\right) - \Delta\cdot\left(n_e \chi_e \frac{dT_e}{d\rho}\right) + \Delta\cdot\left(v_e T_e\right) = S_e \qquad (1)$$

where ρ is the normalized toroidal flux, and v_e and S_e is the radial electron velocity and the source term, respectively. For the continued detachment case (with high gas puff), the pedestal χ_e continuously increases during the whole detachment and the later 3D field application phases. It shows the same trend during the detachment phase, *i.e.* χ_e rises, in the low gas puff case, but comes back down when the 3D fields are applied and the divertor re-attachment occurs. This result is consistent with the T_e profile data shown in figure 4. It is not yet understood why, under this condition, the 3D fields lead to reduced χ_e and higher T_e in the edge region.

One might interpret the dip in the T_e profile shown in figure 4 as a phenomenon associated with island formed in the respective radial location. However, when islands are formed in NSTX, it is usually accompanied by a flat spot at the radial location of the island in T_i and V_t profiles, measured by CHERS, as well as in the T_e and p_e profile [16,17], but in the cases presented in this paper there is no such a spot in either the T_i or V_ϕ profile. Thus we believe the T_e drop here is not related to the island formation.

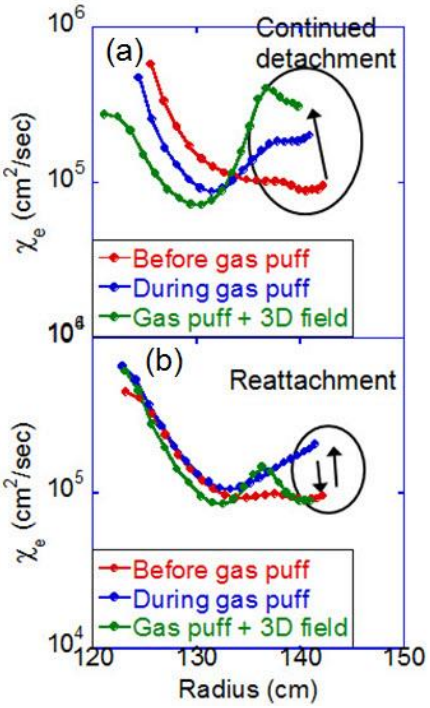

Figure 6 Evolution of pedestal χ_e profile from TRANSP modelling in NSTX for (a) high and (b) low divertor gas puff with 3D fields applied later during the detached phase.

4. Role of plasma response in separatrix splitting and detachment at DIII-D

A similar experiment to look into the effect of 3D fields on divertor detachment was performed at DIII-D in the fall of 2013. A low triangularity plasma shape was chosen in order to locate the outer strike point on the shelf to allow for full diagnostic data from the divertor Thomson scattering (DTS) and IR camera. However, this shape turned out inducing very weak plasma response due to the low kink response. Consequently, there was no strike point splitting from the IR heat flux profile observed for the n=3 even parity and only a subtle, but

persistent, splitting was observed for the odd parity. Figure 7 shows an example of heat flux profile for each case. Since the weak or no strike point splitting by applied 3D fields represents weak 3D response, it is not surprising that the divertor detachment was not affected by 3D fields. Since the causal relationship is now better understood following the data analysis of these discharges, a follow-up experiment to be performed later in 2014 will focus on the effect of plasma shape and collisionality on the plasma response and the divertor plasma regime.

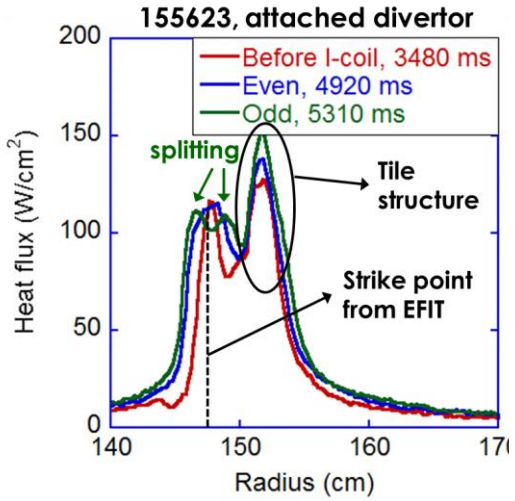

Figure 7: Measured heat flux profiles before 3D fields are applied (red) and with 3D fields for even (blue) and odd (green) parity in DIII-D

The next step is to look into the effect of this resonant and non-resonant plasma response on the strike point splitting. A 3D SOL/divertor transport calculation using a code such as EMC3-Eirene will be necessary to compare to the experiment, but at this stage we just seek for the field line tracing calculation to look at the divertor footprints. Figure 8(a) and 8(b) show the results from a field line tracing using the POCA code [18], for vacuum and ideal plasma response (IPEC) case [19], respectively. This shot had n=3 odd parity perturbation applied and there was clear strike point splitting observed for both heat and particle flux profiles. The vacuum field line tracing exhibits almost no splitting, figure 8(a). However, when plasma response is included in the field line tracing, the splitting is amplified and becomes substantially stronger, which is consistent with the strong kink response observed in the poloidal spectra plot. Indeed this result reflects the experimental observation of clear splitting for this shot, consistent with the amplification of splitting. Note that the footprint pattern from field line tracing does not include any transport effect, but is a pure representation of magnetic lobe structure induced by applied 3D fields. Thus this result indicates that magnetic separatrix splitting is strongly affected by plasma response, without which one could be led to an incorrect result. Another important conclusion from figures 7 and 8 is that the separatrix splitting is not affected only by resonant components, but non-resonant components also play a crucial role.

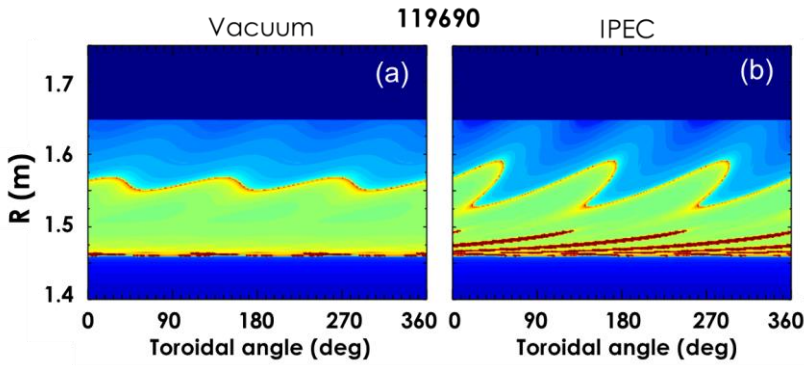

Figure 8 Divertor footprints from a field line tracing in POCA [18] for (a) vacuum and (b) ideal plasma response (IPEC) case for an n=3 odd parity perturbation in DIII-D

From the present data analysis, there expected to be two possibilities regarding the impact of 3D fields on high density divertor plasmas, *i.e.* detached condition. The first one is that the enhanced parallel transport due to the short connection length field lines might cause re-attachment of detached plasma since the lobes contain both long and short connection length field lines. The second possibility is that the counter-streaming flows could lead to

severe momentum loss at the downsteam and the consequent pressure drop might induce enhanced divertor detachment at higher divertor electron temperature than in the axisymmetric condition, as is observed in stellerators [7]. In fact, these two factors are expected to compete and it is yet unclear which one will be more dominant.

Acknowledgements

This work was supported by the US Department of Energy, contract numbers DE-AC05-00OR22725 (ORNL), DE-AC02-09CH11466 (PPPL), DE-FC02-04ER54698 (GA), DE-AC52-07NA27344 (LLNL), and DE-FG02-05ER54809 (UCSD).

References

[1] J.-W. Ahn et al, Phys. Plasmas **18** (2011) 056108

[2] T.W. Petrie et al, Nucl. Fusion **51** (2011) 073003

[3] T.E. Evans et al, Contrib. Plasma Physics **44** (2004) 235

[4] P.C. Stangeby, The Plasma Boundary of Magnetic Fusion Devices, Institute of Physics Pub., Bristol; Philadelphia, 2000

[5] A. Wingen et al, Phys. Plasmas **16** (2009) 042504

[6] O. Schmitz et al, J. Nucl. Mater. **438** (2013) S194

[7] Y. Feng et al, Plasma Phys. Control. Fusion **53** (2011) 024009

[8] V.A. Soukhanovskii et al, Nucl. Fusion **49** (2009) 095025

[9] V.A. Soukhanovskii et al, Rev. Sci. Instrum. **81** (2010) 10D723

[10] J.M. Canik et al, Phys. Rev. Lett. **104** (2010) 045001

[11] J.M. Canik et al, Nucl. Fusion **50** (2010) 034012

[12] J.M. Canik et al, Nucl. Fusion **52** (2012) 054004

[13] S.P. Hirshman et al, Phys. Plasmas **18** (2011) 062504

[14] T.E. Evans et al, J. Physics: Conf. Series **7** (2005) 174

[15] R.J. Hawryluk, Physics of Plasmas Close to Thermonuclear Conditions (Pergamon, Oxford, 1980), Vol. 1, p. 19

[16] J.E. Menard et al, Nucl. Fusion **45** (2005) 539

[17] K.L. Wong et al, Bulletin of the 53rd APS-DPP Annual Meeting, Salt Lake City, USA, 2011 (http://flux.aps.org/meetings/YR11/DPP11/all_DPP11.pdf)

[18] K. Kim et al, Phys. Plasmas **19** (2012) 082503

[19] J.-K. Park et al, Phys. Plasmas **14** (2007) 052110